(Received 31 October 2023, Accepted 10 January 2024, Scheduled 23 January 2024)

An Ultra-Wideband Antenna Based on Left-Handed Materials for IoT Applications

Jincheng Xue[1], Ao Ni[2], Lanzheng Liu[1], Zhuopeng Wang[1], and Xia Wang[3,*]

[1] College of Electronic and Information Engineering, Shandong University of Science and Technology, Qingdao, China
[2] College of Ocean Science and Engineering, Shandong University of Science and Technology, Qingdao, China
[3] Electrical Information Department, Shandong University of Science and Technology, Jinan, China

ABSTRACT: In this paper, a new UWB antenna for the Internet of Things (IoT) based on a left-handed structure is designed. The antenna utilizes a microstrip feeder and consists of a new complementary split ring resonator (CSRR) equipped with a three-stage double rectangular electromagnetic resonator (RER) to form the main radiator with left-handed characteristics. It also includes a double L-shaped parasitic patch and a slotted ground. The dimensions of the antenna are $0.42 \times 0.42 \times 0.013\lambda_0^3$. It covers the frequency band of 1.70–3.34 GHz (65.1%), which includes the communication frequency bands used by IoT antennas. The antenna exhibits good directional patterns within this frequency band. The measured peak gain is 5.49 dBi, making it suitable for applications in Wi-Fi, Bluetooth, Zigbee technology, and other fields.

1. INTRODUCTION

With the rapid development of IoT and modern communication technologies, the design requirements for antennas in IoT applications are becoming increasingly demanding. Due to the fundamental limitations associated with small electrical antennas, finding the optimal antenna design for any wireless system remains a challenge for researchers [1]. Ultra-wideband (UWB) is one of the leading wireless technologies in antenna design, with its advantages of low transmitting power and strong penetration making it suitable for a variety of applications. Compared to other bandwidths, UWB can maintain relatively low power consumption, and its large bandwidth makes it suitable for short-range, high-bandwidth communication in most radio frequency spectra.

Ultra-wideband short-range wireless communication systems have the advantages of effectively reducing spectrum resource occupation, low cost, and stable matching, making UWB antennas increasingly popular among researchers [2]. In [3], a UWB MIMO antenna was designed using two open L-shaped slot antenna elements. The antenna achieved an impedance bandwidth of over 3.1–10.6 GHz, making it suitable for portable UWB applications. In [4], a novel shovel-shaped UWB antenna with three notches was designed, using a hooked defect ground and a loading semi-octagonal resonant ring to achieve three notched frequency bands, resulting in an impedance bandwidth of 2.9–13 GHz. In [5], researchers designed a UWB antenna for medical microwave imaging (MWI) applications. The butterfly-shaped antenna's cross arms were connected perpendicularly to a UWB balun, achieving UWB performance from 1 to 6 GHz. This makes the antenna suitable for more precise, multi-frequency MWI systems and can be used in UWB-MWI hybrid systems. A UWB antenna system for cognitive radio was proposed, integrated with a slot line-based MIMO antenna and a quadrupole half-ring UWB MIMO antenna system on the same substrate [6]. The antenna covers a frequency range of 1.48–4.56 GHz, suitable for UWB-MIMO systems.

Left-handed metamaterials have received widespread attention in antenna design due to their unique electromagnetic properties. Left-handed metamaterials can reduce antenna resonant frequency, resulting in miniaturization [7, 8], increase antenna bandwidth [9–13], gain [14, 15], and improve antenna radiation efficiency [16, 17]. In [18], a composite metamaterial consisting of an inner open-ring resonator and an outer closed-ring resonator was proposed, achieving dual-band operation in the frequency ranges of 2.595–2.654 GHz and 3.185–4.245 GHz through two resonant modes. A wheel-shaped metamaterial was proposed, with linearly polarized patches placed on the metasurface to achieve circular polarization [19]. In [20], a novel three-layer annular metamaterial absorber (MA) was proposed and arranged into a double-ring structure, effectively reducing the radar cross section inside the band.

The purpose of the paper is to design a UWB antenna with left-handed structure characteristics. The authors achieve this by loading a three-stage double RERs into the CSRR to form the main radiator of the antenna. This structure enables the antenna to have left-handed radiation characteristics. The ground slot not only reduces the reflection interference of the ground to the antenna, but also increases the matching degree of the antenna to ensure the left-handed characteristics of the antenna. The designed antenna operates within the frequency range of 1.70–3.34 GHz, which covers the 1800 MHz, 900 MHz, 2.4 GHz, and other bands commonly used in the IoT applications. The paper validates the effectiveness and usability of the antenna through physical tests.

* Corresponding author: Xia Wang (skd992370@sdust.edu.cn).

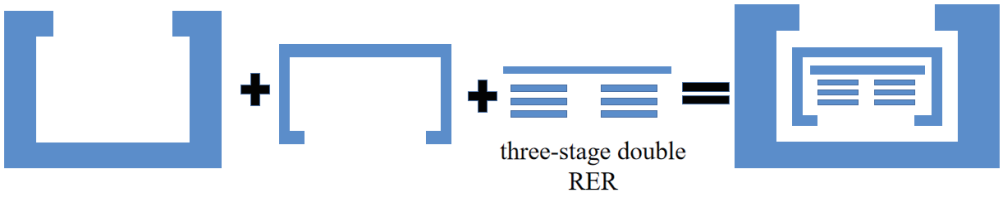

FIGURE 1. Schematic diagram of left-hand structure.

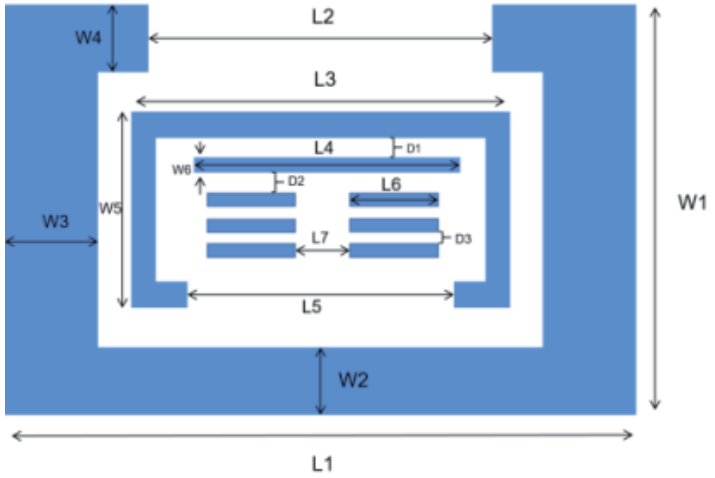

FIGURE 2. Schematic diagram of antenna dimensions.

TABLE 1. Size parameters of left-handed metamaterial structure.

Parameters	Value/mm	Parameters	Value/mm	Parameters	Value/mm
W_1	26	W_4	4	L_7	4
L_1	40	L_4	18	D_1	2
W_2	4	W_5	14	D_2	1
L_2	22	L_5	18	D_3	1
W_3	6	W_6	1		
L_3	24	L_6	6		

2. LEFT-HANDED STRUCTURE DESIGN

It is correct that the paper proposes a novel left-handed structure. The structure consists of a reverse opening ring loaded inside the opening ring to form the complementary split ring resonator (CSRR). Inside the CSRR, a three-stage double rectangular electromagnetic resonator (RER) is loaded to create a new left-handed structure. This structure is printed on an FR4 medium substrate. Figure 2 shows a schematic diagram of the left-handed structure. The size data for the left-handed structure are provided in Table 1. The port settings of the left-handed structure simulation model are shown in Figure 3(a): the upper and lower parts are prefect H; the left and right parts are wave port; and the front and rear parts are prefect E. This is done so that the electric field is parallel to the patch, and the magnetic field is perpendicular to the patch, which can simulate the periodic structure. The left-handed structure was simulated on a 1.6 mm thick FR-4 substrate. The results, as shown in Figure 3(b), demonstrate that the amplitude and phase of S_{11} of the structure undergo changes around 2 GHz within the working bandwidth.

This section describes the analysis and optimization of the equivalent circuit model for the left-handed structure using advanced design system (ADS). Figure 4 presents the equivalent circuit diagram obtained through the ADS assignment optimization of each component. The component assignments are provided in Table 2. The three ring circuits of the equivalent circuit respectively represent the three-layer structure of the antenna, in which L_1–L_6 and C_1–C_6 are the capacitors and inductors introduced in the RER; C_7, C_9, and C_{10} are the coupling capacitors generated between the RER and the inner and outer opening rings; L_8–L_{12} are the ring inductors generated by the inner and outer opening rings; C_8 and C_{11} are capacitors generated at the opening of two open rings. Additionally, Figure 5 displays the amplitude and phase characteristics obtained through the simulation of the equivalent circuit model in ADS. The analysis reveals that the equivalent circuit model exhibits two phase break points at 2 GHz, which aligns with the

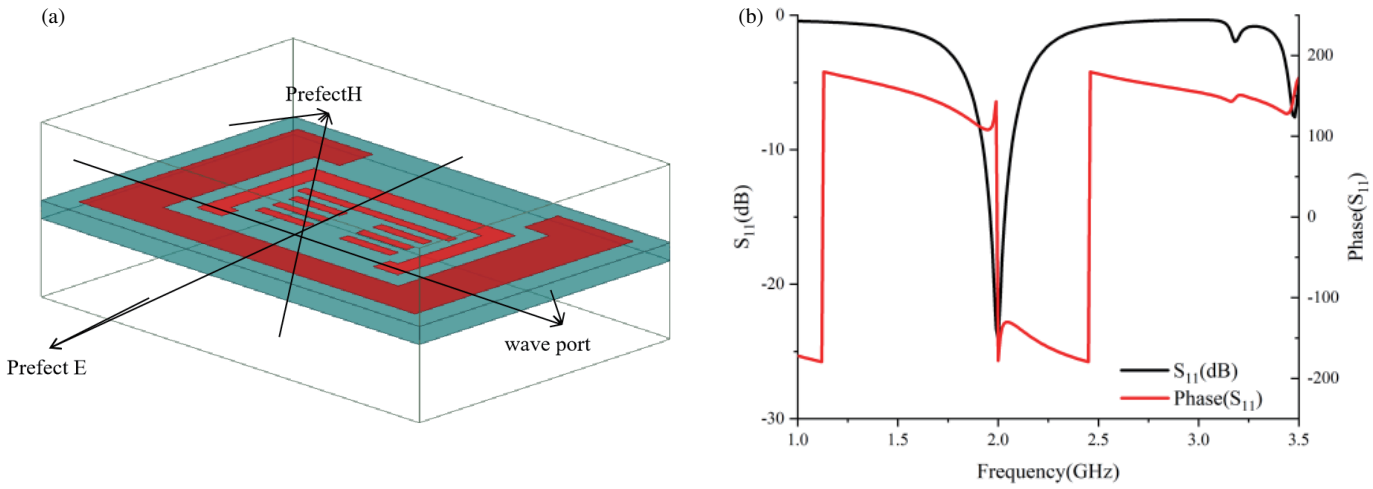

FIGURE 3. Left-handed structure, (a) simulation model, (b) simulation result.

TABLE 2. Equivalent circuit element assignment.

Parameters	Value	Parameters	Value	Parameters	Value
C_1	1 pF	C_9	1.1 pF	L_6	1 nH
C_2	1 pF	C_{10}	1.1 pF	L_7	1.2 nH
C_3	1 pF	C_{11}	0.01 pF	L_8	1.5 nH
C_4	1 pF	L_1	1 nH	L_9	0.55 nH
C_5	1 pF	L_2	1 nH	L_{10}	0.55 nH
C_6	1 pF	L_3	1 nH	L_{11}	3 nH
C_7	15 pF	L_4	1 nH	L_{12}	3 nH
C_8	1.6 pF	L_5	1 nH	L_{13}	4.5 nH

phase characteristics observed in the electromagnetic simulation of the left-handed structure.

The equivalent electromagnetic parameters of the left-handed metamaterial structure can be obtained by inversion of the S-parameter, and its equivalent permittivity, effective permeability, and wave impedance can be obtained. The parameter inversion algorithm [21] can be expressed as

$$\varepsilon = \frac{n_e}{z} \tag{1}$$

$$\mu = n_e z \tag{2}$$

$$n_e = \frac{1}{kh}\cos^{-1}\frac{1-S_{11}^2+S_{21}^2}{2S_{21}}+\frac{2\pi u}{kd} \tag{3}$$

$$z = \pm\sqrt{\frac{(1+S_{11})^2-S_{21}^2}{(1-S_{11})^2-S_{21}^2}} \tag{4}$$

where ε is the effective dielectric constant; n_e is the effective refractive index; z is the wave impedance; μ is the effective permeability; k is the wave number; h is the thickness of metamaterial; S_{11} and S_{21} are scattering parameters; u is an integer that represents the branch of the inverse cosine function. Figure 6 shows the equivalent permittivity, equivalent permeability, refractive index, and wave impedance after parameter inversion. As can be seen from Figure 6, the equivalent permittivity of the left-handed metamaterial structure is negative in 1.7–3.55 GHz, including all operating bandwidths; the equivalent permeability is negative in 1.9–2.74 GHz; and the refractive index is negative in 1.8–3.32 GHz, realizing the left-handed characteristic in the operating bandwidths.

3. ANTENNA DESIGN

The antenna was designed on an FR-4 dielectric substrate with a thickness of 1.6 mm, a dielectric constant of 4.4, and a loss tangent of 0.02. Figure 7 illustrates the configuration and geometry of the antenna, which includes an entire radiator with a simple feeder, a double "L" type parasitic patch, and left-handed characteristics (as shown in Figure 1), a substrate, and a slotted ground. In the figure, the blue represents the upper antenna radiation structure, the yellow represents the ground, and the green represents the slot. The specific size parameters of the antenna are listed in Table 3.

$$W_g = 0.083 \cdot \frac{c}{f_0\sqrt{\varepsilon_r}} \tag{5}$$

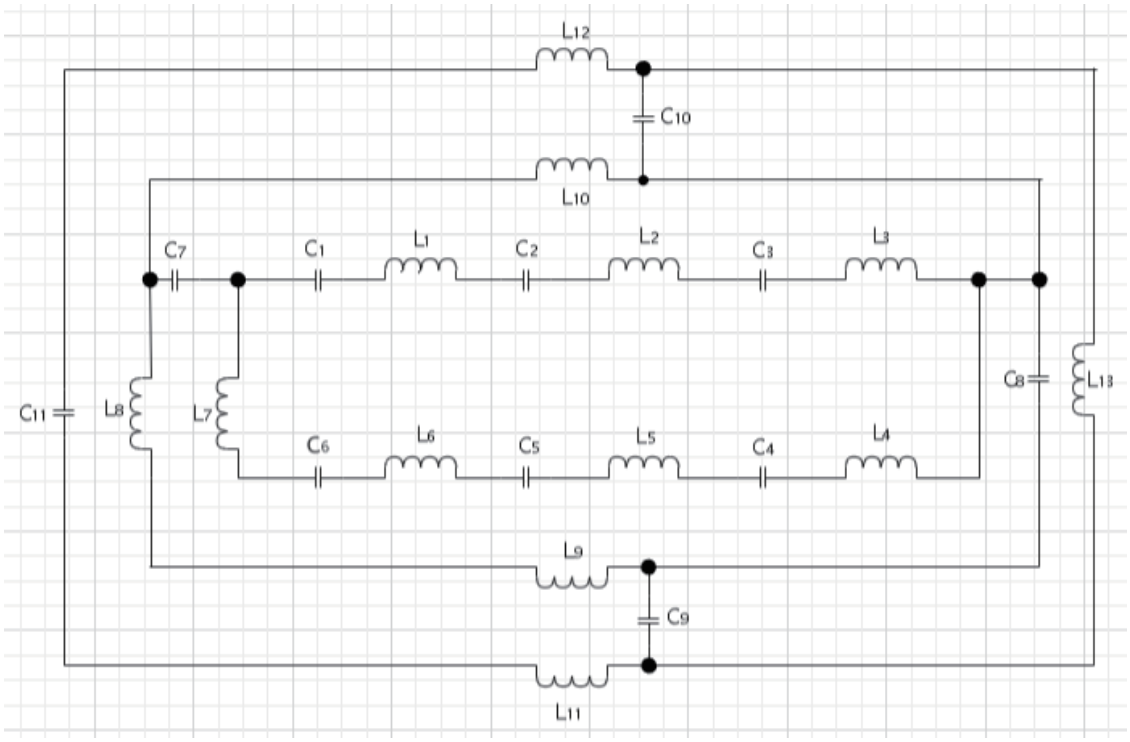

FIGURE 4. Equivalent circuit diagram of left-handed structure.

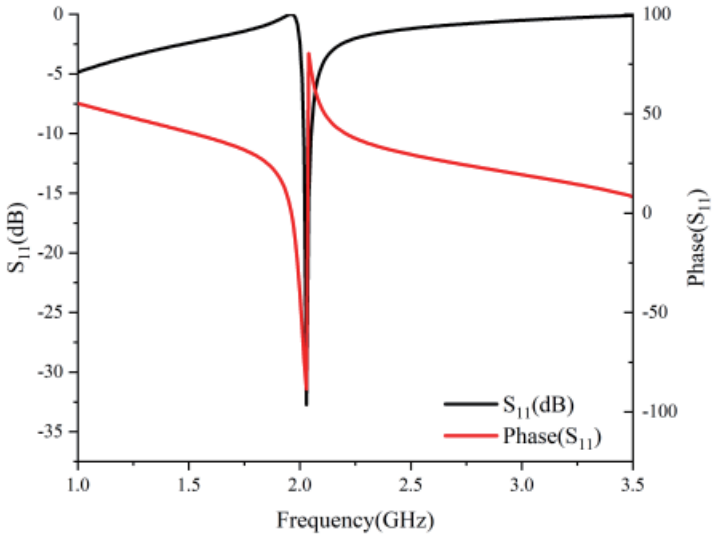

FIGURE 5. Simulation result of in ADS.

TABLE 3. Antenna size parameters (unit: mm).

Parameters	Unit/mm	Parameters	Unit/mm
W	50	W_g	18
L	50	L_g	17
W_s	30	W_s	1
L_s	44	L_s	9
D_4	1.1		

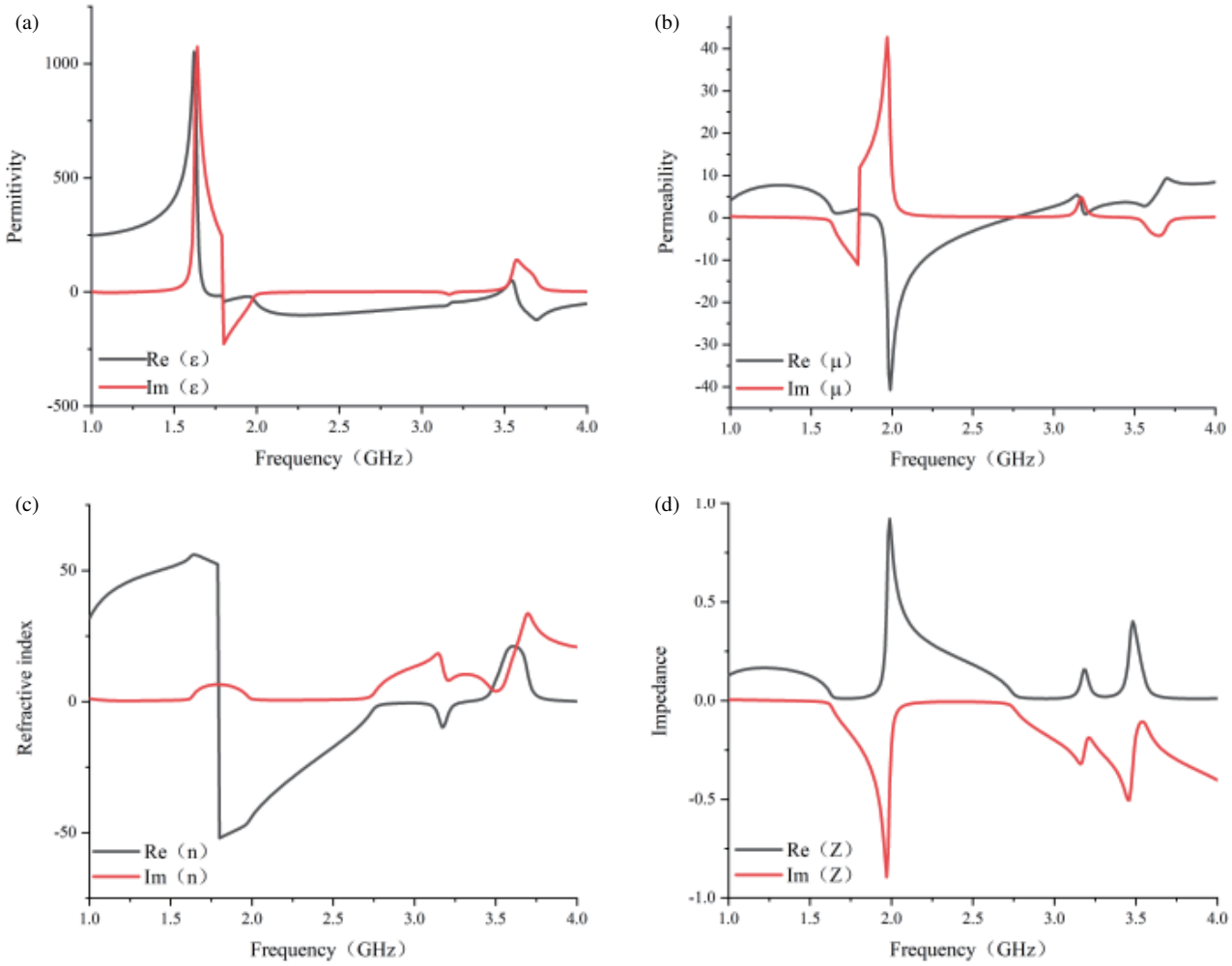

FIGURE 6. S-parameter inversion. (a) Equivalent permittivity. (b) Equivalent permeability. (c) Refractive index. (d) Impedance.

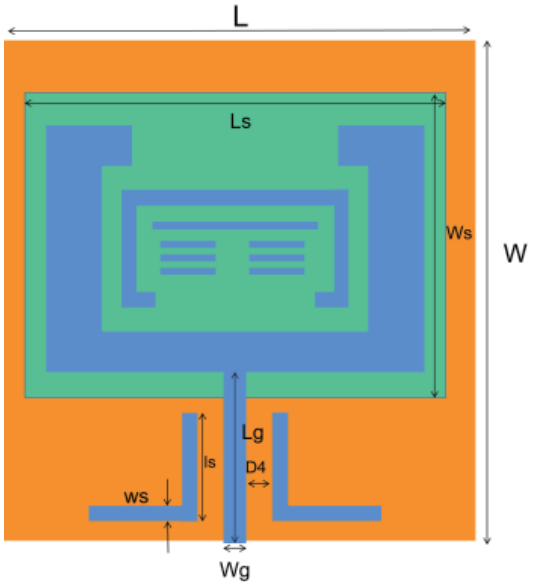

FIGURE 7. Antenna structure.

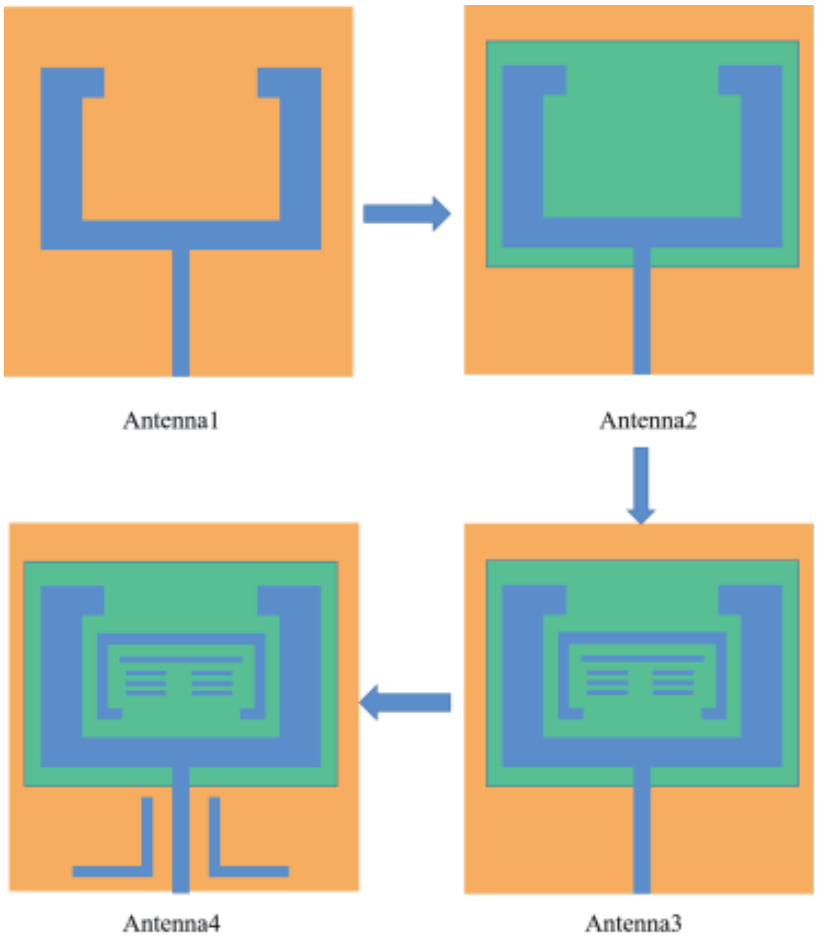

FIGURE 8. Antenna design process.

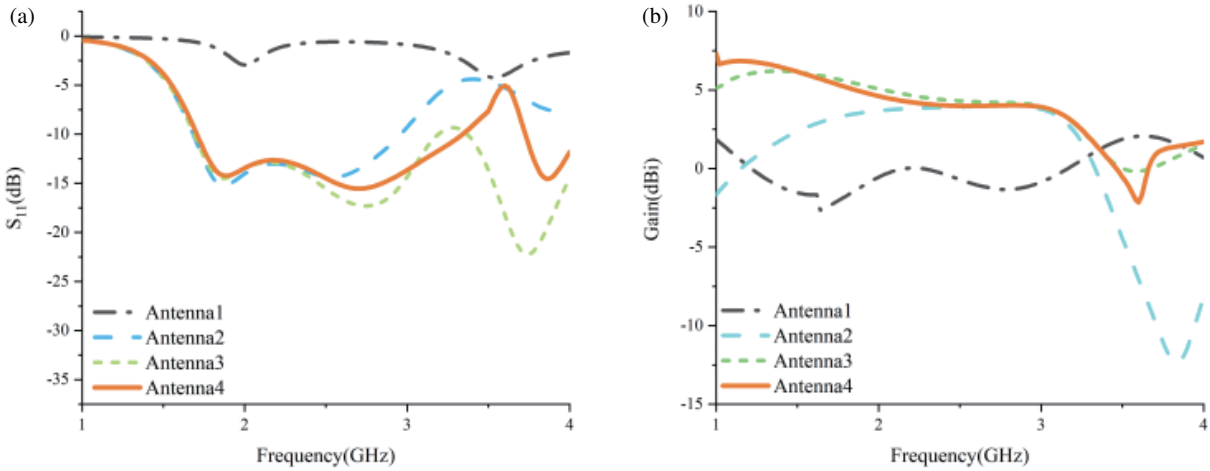

FIGURE 9. Antenna performance comparison (a) impedance bandwidth (b) gain.

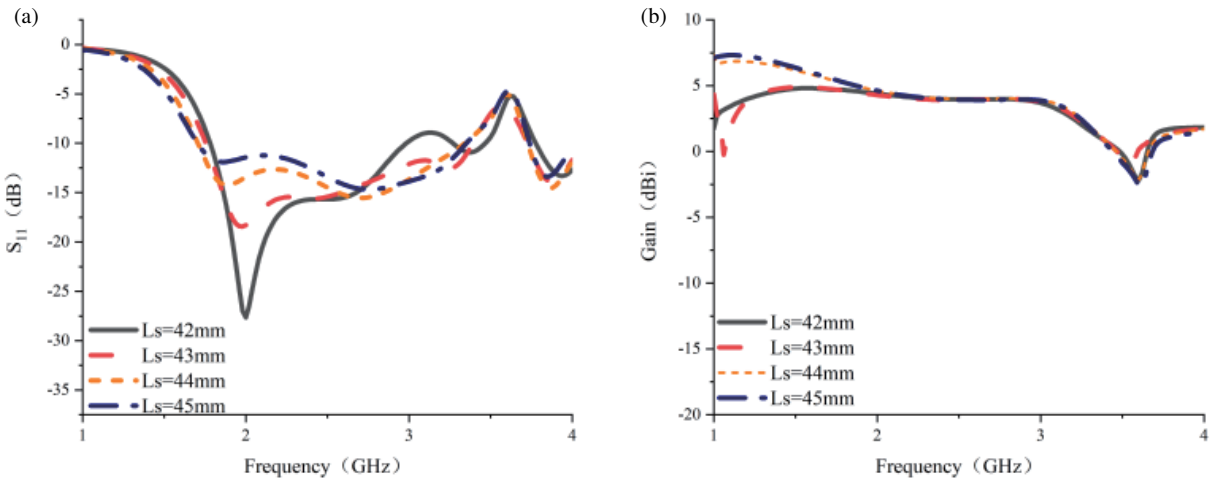

FIGURE 10. Influence of parameter L_s on antenna performance (a) impedance bandwidth (b) gain.

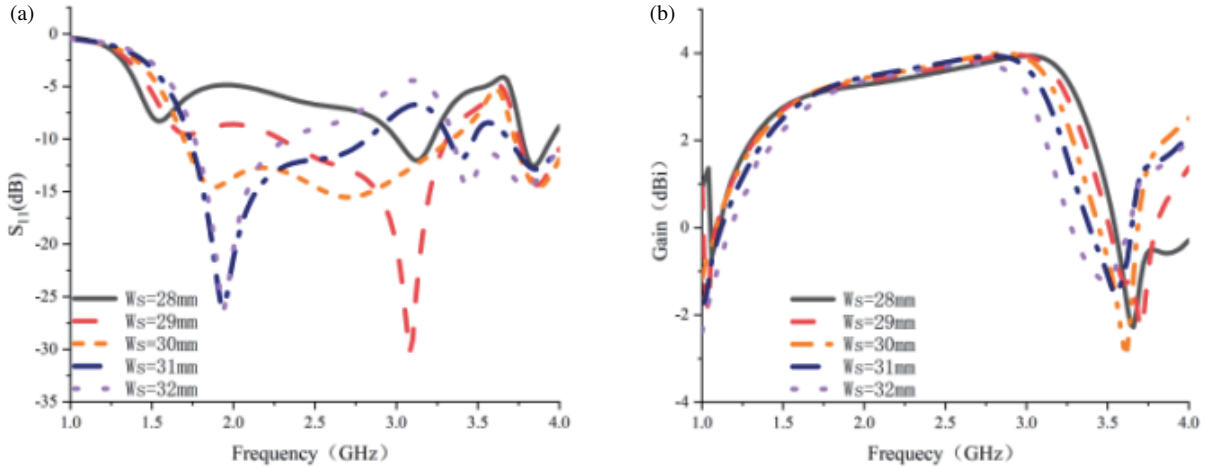

FIGURE 11. Influence of parameter D_4 on antenna performance (a) impedance bandwidth (b) gain.

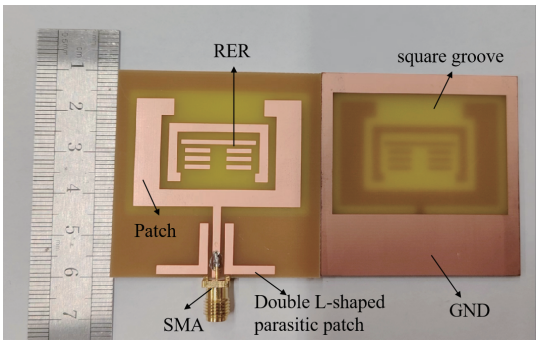

FIGURE 12. Antenna physical diagram.

$$L_g = \frac{c}{2f_0\sqrt{\varepsilon_r}} \tag{6}$$

Formulas (5) and(6) are the relationship between the width and length of the feeder and the resonant frequency of the antenna, respectively. c is the speed of light in vacuum, f_0 the resonant frequency of the antenna, and ε_r the effective dielectric constant of the substrate.

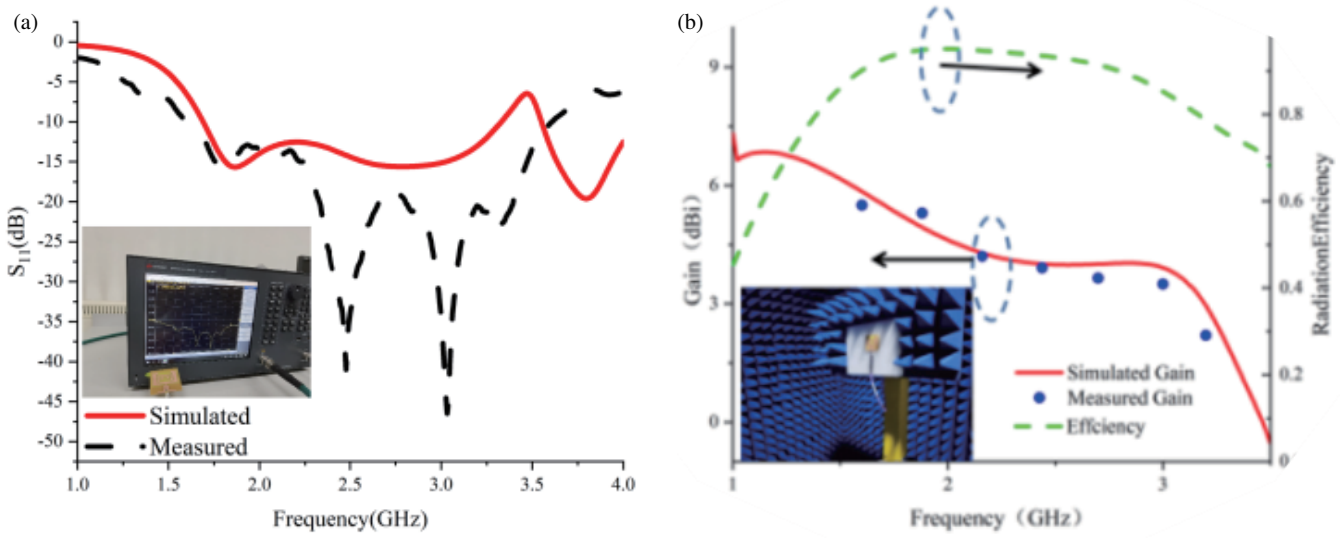

FIGURE 13. Simulated and measured results. (a) S_{11}. (b) Gain, efficiency.

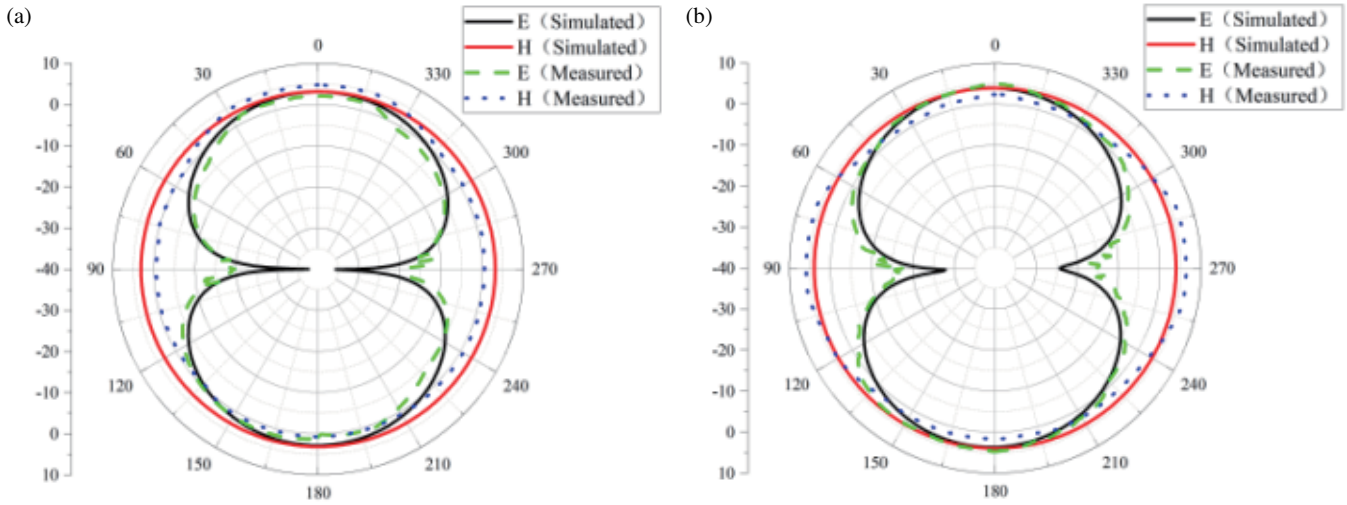

FIGURE 14. Simulated and measured results of radiation pattern. (a) 1.88 GHz, (b) 2.7 GHz.

The antenna design is depicted in Figure 8. To begin, we designed a monopole open loop antenna, referred to as Antenna 1, which is fed through a microstrip feeder. In the next step, we modified the ground by adding slots to create Antenna 2. Subsequently, we incorporated complementary open rings and a three-stage double rectangular electromagnetic resonator to fashion Antenna 3. The ultimate Antenna 4 was realized by introducing parasitic double L-shaped patches on both sides of the feeder. Figure 9 illustrates the performance characteristics of these four antennas at various stages of the design process.

As observed in Figure 9, Antenna 1 exhibited poor impedance matching, generating only a single resonance point at 2 GHz. Antenna 2, with a ground square slot, was designed. This led to a reduction in the impact of multipath interference, enhancing the signal quality and reliability, and significantly improving antenna matching. Antenna 2 extended the operating bandwidth from 1.68 to 2.96 GHz, accompanied by a notable gain increase. Subsequently, we introduced a reverse-opening ring and a three-stage double rectangular electromagnetic radiator at the core of the monopole antenna. Together, they created a left-handed structure and increased the impedance bandwidth of the antenna. The impedance bandwidth was expanded to 1.69–3.19 GHz, and the gain in the lower band increased by approximately 2 dBi. Certainly, the inclusion of double "L" shaped patches as parasitic elements on both sides of the feeder in Antenna 4 significantly influences the antenna's electromagnetic characteristics. By strategically adjusting the position and size of these parasitic patches, the impedance bandwidth of the antenna experiences a notable expansion. As a result, the final antenna impedance bandwidth reaches 1.7–3.34 GHz, indicating a substantial enhancement over the initial design. Moreover, the gain of Antenna 4 experiences a remarkable improvement of approximately 5 dBi in comparison to the performance of Antenna 1.

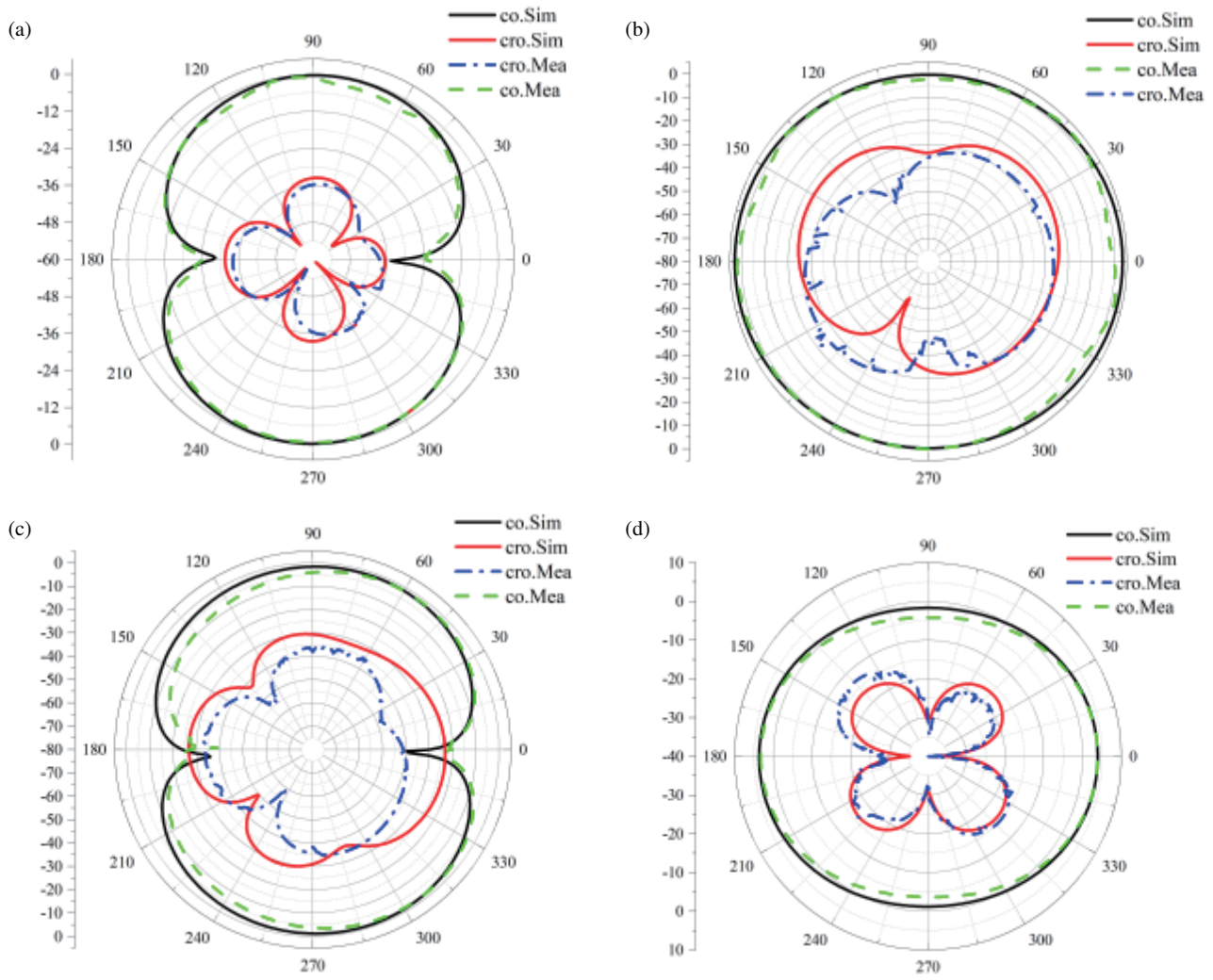

FIGURE 15. Cross-polarization, (a) E-plane at 1.88 GHz, (b) H-plane at 1.88 GHz, (c) E-plane at 2.7 GHz, (d) H-plane at 1.88 GHz.

4. PARAMETRIC RESEARCH

Figures 10 and 11 show that changing the width (W_s) and length (L_s) of the square slot has a significant impact on the antenna's performance. This is expected because the ground square slot is an integral part of the antenna structure, and its dimensions influence how the antenna radiates and receives electromagnetic waves. Alterations in L_s and W_s can affect not only the antenna's radiation but also the interference and reflection of electromagnetic waves by the ground. This, in turn, affects the overall electromagnetic characteristics of the antenna.

We investigated a range of values for L_s and W_s. The length L_s varied between 42 mm and 45 mm, while the width W_s ranged from 28 mm to 32 mm. As can be seen in Figure 10, when L_s continues to increase, the antenna impedance bandwidth and gain are slightly increased. When L_s reaches 45 mm, the antenna impedance matching becomes worse, and the bandwidth begins to narrow, so $L_s = 44$ mm is selected. As can be seen from Figure 11, with the increase of W_s, the antenna impedance bandwidth becomes larger, and the resonance begins to move forward. When the bandwidth is 31 mm, the impedance bandwidth of a higher frequency band begins to be lost, and the gain change is not obvious, so $W_s = 30$ mm is selected. These values provided the desired impedance bandwidth and gain, indicating that this combination of L_s and W_s meets the antenna design objectives.

5. SIMULATION AND MEASUREMENT

The S_{11}, gain, and radiation efficiency of the antenna were determined through electromagnetic simulation software. Subsequently, the designed antenna was fabricated and rigorously tested, corroborating the simulation results. In Figure 12, we present actual images of the antenna from both the front and back. In Figure 13(a), a comparison is made between the simulated and measured S_{11} parameters of the antenna. The measured impedance bandwidth ranges from 1.61 GHz to 3.60 GHz. Compared with the simulation value, the bandwidth is slightly increased, and the antenna matching degree is stronger. This observation suggests a high degree of alignment between the design expectations and the real-world performance of the antenna. Moreover, when evaluating the gain

TABLE 4. Performance comparison between this design and other antennas.

Reference	Overall dimension (λ_0^3)	$S_{11} < -10$ dB (GHz)	Gain (dBi)	-10 dB Bandwidth (%)
[22]	$0.23 \times 0.23 \times 0.04$	0.896–0.958	2.4	6.7
[23]	$0.7 \times 0.47 \times 0.084$	1.62–2.78	6	52.7
[24]	$0.28 \times 0.28 \times 0.042$	2.42–2.5	1.2	2.4
[25]	$0.75 \times 0.75 \times 0.027$	2.3–2.53/ 5.63–5.95	4.88/4.73	9.6/12.4
This work	$0.42 \times 0.42 \times 0.013$	1.70–3.34	5.49	65.1

across the entire frequency band, we find that the measured results largely meet the antenna's design specifications. Although there is a minor reduction in radiation efficiency in the higher frequency range, it consistently exceeds 75%, signifying a notably high radiation efficiency.

In Figure 14, the antenna patterns at 1.88 GHz and 2.7 GHz are displayed, showing a comparison between the simulated and measured results. Notably, there is a consistent alignment between the simulated and measured patterns at these frequencies, indicating the reliability of the simulation model. This consistency between simulation and measurement enhances the credibility of the antenna design and its expected performance. Furthermore, the study includes a comparative analysis with other antennas utilized in Internet of Things (IoT) applications. The results of this comparison are presented in Table 4. Figure 15 shows the polarization pattern of the antenna at 1.88 GHz and 2.7 GHz. It can be seen that the antenna is cross-polarized. Although the measured antenna is slightly offset, it is in good agreement with the simulation.

6. SUMMARY

In this paper, we propose a left-handed UWB antenna for IoT applications. A new type of left-handed CSRR antenna equipped with three-stage double RER is designed. Through the ground slotted technology, the matching degree of the antenna is increased, which provides electromagnetic environment for the left-handed structure. The double L-shaped parasitic patch changes the radiation characteristics of the antenna, increases the impedance bandwidth while maintaining a good gain, and finally makes the antenna achieve ultra-wideband characteristics which has great potential in IoT applications.

REFERENCES

[1] Bekasiewicz, A. and S. Koziel, "Compact UWB monopole antenna for internet of things applications," *Electronics Letters*, Vol. 52, No. 7, 492–494, Apr. 2016.

[2] Zhu, F., S. Gao, A. T. S. Ho, R. A. Abd-Alhameed, C. H. See, T. W. C. Brown, J. Li, G. Wei, and J. Xu, "Multiple band-notched UWB antenna with band-rejected elements integrated in the feed line," *IEEE Transactions on Antennas and Propagation*, Vol. 61, No. 8, 3952–3960, Aug. 2013.

[3] Ren, J., W. Hu, Y. Yin, and R. Fan, "Compact printed MIMO antenna for UWB applications," *IEEE Antennas and Wireless Propagation Letters*, Vol. 13, 1517–1520, 2014.

[4] Li, W. T., X. W. Shi, and Y. Q. Hei, "Novel planar UWB monopole antenna with triple band-notched characteristics," *IEEE Antennas and Wireless Propagation Letters*, Vol. 8, 1094–1098, 2009.

[5] Fiser, O., V. Hruby, J. Vrba, T. Drizdal, J. Tesarik, J. V. Jr, and D. Vrba, "UWB bowtie antenna for medical microwave imaging applications," *IEEE Transactions on Antennas and Propagation*, Vol. 70, No. 7, 5357–5372, Jul. 2022.

[6] Hussain, R. and M. S. Sharawi, "An integrated slot-based frequency-agile and UWB multifunction MIMO antenna system," *IEEE Antennas and Wireless Propagation Letters*, Vol. 18, No. 10, 2150–2154, 2019.

[7] Huang, H., Y. Liu, S. Zhang, and S. Gong, "Multiband metamaterial-loaded monopole antenna for WLAN/WiMAX applications," *IEEE Antennas and Wireless Propagation Letters*, Vol. 14, 662–665, 2015.

[8] Li, M., K.-M. Luk, L. Ge, and K. Zhang, "Miniaturization of magnetoelectric dipole antenna by using metamaterial loading," *IEEE Transactions on Antennas and Propagation*, Vol. 64, No. 11, 4914–4918, Nov. 2016.

[9] Li, K., C. Zhu, L. Li, Y.-M. Cai, and C.-H. Liang, "Design of electrically small metamaterial antenna with ELC and EBG loading," *IEEE Antennas and Wireless Propagation Letters*, Vol. 12, 678–681, 2013.

[10] Zhu, J. and G. V. Eleftheriades, "A compact transmission-line metamaterial antenna with extended bandwidth," *IEEE Antennas and Wireless Propagation Letters*, Vol. 8, 295–298, 2009.

[11] Ameen, M. and R. K. Chaudhary, "Metamaterial-based wideband circularly polarised antenna with rotated V-shaped metasurface for small satellite applications," *Electronics Letters*, Vol. 55, No. 7, 365–366, Apr. 2019.

[12] Liu, P., W. Jiang, S. Sun, Y. Xi, and S. Gong, "Broadband and low-profile penta-polarization reconfigurable metamaterial antenna," *IEEE Access*, Vol. 8, 21 823–21 831, 2020.

[13] Hasan, M. M., M. R. I. Faruque, and M. T. Islam, "Thin-layer dielectric and left-handed metamaterial stacked compact triband antenna for 2 GHz to 4 GHz wireless networks," *Journal of Electronic Materials*, Vol. 48, 3979–3990, 2019.

[14] Shi, X., Y. Cao, Y. Hu, X. Luo, H. Yang, and L. H. Ye, "A high-gain antipodal Vivaldi antenna with director and metamaterial at 1–-28 GHz," *IEEE Antennas and Wireless Propagation Letters*, Vol. 20, No. 12, 2432–2436, 2021.

[15] Li, Y. and J. Chen, "Design of miniaturized high gain bowtie antenna," *IEEE Transactions on Antennas and Propagation*, Vol. 70, No. 1, 738–743, Jan. 2022.

[16] Ha, J., K. Kwon, Y. Lee, and J. Choi, "Hybrid mode wideband patch antenna loaded with a planar metamaterial unit cell," *IEEE Transactions on Antennas and Propagation*, Vol. 60, No. 2, 1143–1147, Feb. 2012.

[17] Saghanezhad, S. A. H. and Z. Atlasbaf, "Miniaturized dual-band CPW-fed antennas loaded with U-shaped metamaterials," *IEEE Antennas and Wireless Propagation Letters*, Vol. 14, 658–661, 2014.

[18] Si, L.-M., W. Zhu, and H.-J. Sun, "A compact, planar, and CPW-fed metamaterial-inspired dual-band antenna," *IEEE Antennas and Wireless Propagation Letters*, Vol. 12, 305–308, 2013.

[19] Liu, Y., K. Song, Y. Qi, S. Gu, and X. Zhao, "Investigation of circularly polarized patch antenna with chiral metamaterial," *IEEE Antennas and Wireless Propagation Letters*, Vol. 12, 1359–1362, 2013.

[20] Ren, J., S. Gong, and W. Jiang, "Low-RCS monopolar patch antenna based on a dual-ring metamaterial absorber," *IEEE Antennas and Wireless Propagation Letters*, Vol. 17, No. 1, 102–105, Jan. 2018.

[21] Smith, D. R., D. C. Vier, T. Koschny, and C. M. Soukoulis, "Electromagnetic parameter retrieval from inhomogeneous metamaterials," *Physical Review E*, Vol. 71, Mar. 2005.

[22] An, W., X. Wang, H. Fu, J. Ma, X. Huang, and B. Feng, "Low-profile wideband slot-loaded patch antenna with multiresonant modes," *IEEE Antennas and Wireless Propagation Letters*, Vol. 17, No. 7, 1309–1313, Jul. 2018.

[23] Oh, J.-I., H.-W. Jo, K.-S. Kim, H. Cho, and J.-W. Yu, "A compact cavity-backed slot antenna using dual mode for IoT applications," *IEEE Antennas and Wireless Propagation Letters*, Vol. 20, No. 3, 317–321, Mar. 2021.

[24] Ahmad, S., K. N. Paracha, Y. A. Sheikh, A. Ghaffar, A. D. Butt, M. Alibakhshikenari, P. J. Soh, S. Khan, and F. Falcone, "A metasurface-based single-layered compact AMC-backed dual-band antenna for off-body IoT devices," *IEEE Access*, Vol. 9, 159 598–159 615, 2021.